

# Charge ordering modulations in a $\text{Bi}_{0.4}\text{Ca}_{0.6}\text{MnO}_3$ film with a thickness of 110 nm\*

Ding Yan-Hua(丁艳华)<sup>a)b)</sup>, Wang Yi-Qian(王乙潜)<sup>a)†</sup>, Cai Rong-Sheng(蔡镛声)<sup>a)b)</sup>,  
Chen Yun-Zhong(陈允忠)<sup>c)</sup>, and Sun Ji-Rong(孙继荣)<sup>c)</sup>

<sup>a)</sup>The Cultivation Base for State Key Laboratory, Qingdao University, Qingdao 266071, China

<sup>b)</sup>College of Chemistry, Chemical Engineering and Environmental Engineering,  
Qingdao University, Qingdao 266071, China

<sup>c)</sup>State Key Laboratory of Magnetism and Beijing National Laboratory for Condensed Matter Physics,  
Institute of Physics, Chinese Academy of Sciences, Beijing 100190, China

(Received 21 March 2012; revised manuscript received 25 April 2012)

The low temperature sample stage in a transmission electron microscope is used to investigate the charge ordering behaviours in a  $\text{Bi}_{0.4}\text{Ca}_{0.6}\text{MnO}_3$  film with a thickness of 110 nm at 103 K. Six different types of superlattice structures are observed using the selected-area electron diffraction (SAED) technique, while three of them match well with the modulation stripes in high-resolution transmission electron microscopy (HRTEM) images. It is found that the modulation periodicity and direction are completely different in the region close to the  $\text{Bi}_{0.4}\text{Ca}_{0.6}\text{MnO}_3/\text{SrTiO}_3$  interface from those in the region a little further from the  $\text{Bi}_{0.4}\text{Ca}_{0.6}\text{MnO}_3/\text{SrTiO}_3$  interface, and the possible reasons for this are discussed. Based on the experimental results, structural models are proposed for these localized modulated structures.

**Keywords:** charge ordering, selected-area electron diffraction, high-resolution transmission electron microscopy, pulsed laser deposition

**PACS:** 75.25.Dk, 61.05.J-, 68.37.Og, 81.15.Fg **DOI:** 10.1088/1674-1056/21/8/087502

## 1. Introduction

The charge ordering state in perovskite manganite has attracted a lot of interest because of its unusual magnetic and electronic properties.<sup>[1–4]</sup> In manganite systems, charge ordering (CO) modulation characterized by a periodic arrangement of  $\text{Mn}^{3+}$  and  $\text{Mn}^{4+}$  associated with the  $d_{z^2}$  orbital ordering (OO) can be induced by a cooperative Jahn–Teller distortion of the  $\text{Mn}^{3+}\text{O}_6$  octahedra.<sup>[5–8]</sup> In particular, the CO phenomena in the  $\text{ABO}_3$ -type rare earth manganites with the formula  $\text{Bi}_{1-x}\text{Ca}_x\text{MnO}_3$  has aroused a lot of research interest,<sup>[9–11]</sup> owing to its high CO temperature and associated diverse property anomalies.

Bismuth-based manganites are a special system possessing higher CO/OO transition temperatures than other manganites, well above room temperature in some cases,<sup>[12]</sup> which manifests a strong tendency toward a CO state for the materials. A  $\text{Bi}_{0.4}\text{Ca}_{0.6}\text{MnO}_3$  (BCMO) film with a thickness of

more than 100 nm has a clear CO transition around 260 K. Kim *et al.*<sup>[13]</sup> investigated the CO transitions in the epitaxial BCMO films thicker than 300 nm. Chen *et al.*<sup>[14–16]</sup> systematically studied the effects of lattice strain on the CO transition and the electronic transport properties of BCMO films thinner than 200 nm. However, detailed microstructural information about CO behaviour in BCMO epitaxial films thinner than 200 nm is lacking. Figure 1 shows the CO transition degree as a function of BCMO film thickness. It can be seen that the film with a thickness of 110 nm just transforms into a perfect CO state, and complex CO behaviours and various stripe phases are expected. Therefore, it is worthwhile to perform a careful study on the CO states in a 110-nm-thick BCMO film. In this paper, we investigate the CO transition in the 110-nm-thick BCMO film grown on an  $\text{SrTiO}_3$  (STO) substrate by using transmission electron microscopy (TEM), and the structures of BCMO films at 103 K

\*Project supported by the National Natural Science Foundation of China (Grant Nos. 10974105 and 50832007), the Project of Introducing Talents to Support Thousand Talents Programs, China (Grant No. P201101032), the Program of Upgrading Technology for Scientific Instruments in Shandong Province, China (Grant No. 2011SJZ16), and the Program of Science and Technology in Qingdao City, China (Grant No. 11-2-4-23-hz).

†Corresponding author. E-mail: yqwang@qdu.edu.cn

© 2012 Chinese Physical Society and IOP Publishing Ltd

<http://iopscience.iop.org/cpb> <http://cpb.iphy.ac.cn>

by using selected area electron diffraction (SAED) and high-resolution electron microscopy (HRTEM).

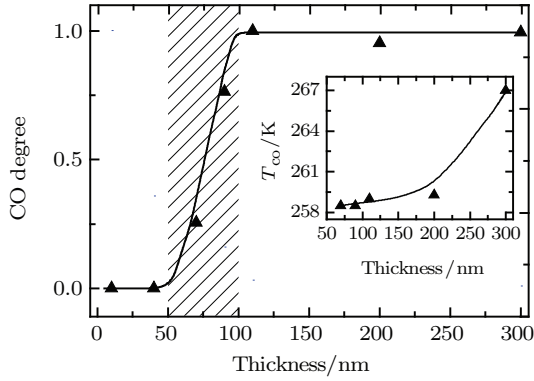


**Fig. 1.** (colour online) The CO transition degree as a function of film thickness. Inset shows the thickness-dependent CO transition temperature  $T_{CO}$ .

## 2. Experiment

Epitaxial BCMO films were prepared on (110) STO substrates by the pulsed laser deposition (PLD) technique (laser wavelength = 248 nm, repetition rate = 5 Hz, and fluency = 7 J/cm<sup>2</sup>) from a target with a nominal composition of BCMO. During the deposition, the substrate temperature was kept at  $\sim 700$  °C and the oxygen pressure at  $\sim 60$  Pa. The film thickness was controlled by the deposition time. Structural analyses of the films were performed by X-ray diffraction (XRD) analysis on a Philips X'pert Pro diffractometer using Cu K $\alpha_1$  radiation.

Specimens for TEM examinations were prepared in a cross-sectional orientation ([ $\bar{1}\bar{1}0$ ] zone-axis for the STO substrate) using conventional techniques of mechanical polishing and ion thinning. The ion milling was performed using a Gatan Model 691 Precision Ion Polishing System (PIPS). A JEOL JEM 2100F transmission electron microscope with low-temperature sample stage was used for SAED and HRTEM imaging. The temperature was set and maintained at 103 K by Gatan SmartSet cold stage controller (636.MA).

## 3. Results and discussion

XRD analysis<sup>[14]</sup> shows that the BCMO film has a pseudo-cubic structure ( $a \approx b \approx c = 3.901$  Å,  $1$  Å = 0.1 nm) at room temperature. Figure 2(a) shows a typical bright field (BF) TEM image of a cross-sectional BCMO/STO sample with a film thickness of

110 nm, recorded at room temperature. The BF image was taken under a two-beam condition with  $g = 110$ . The interface between the BCMO and STO is indicated by two arrows. Figure 2(b) shows a [ $\bar{1}\bar{1}0$ ] zone-axis SAED pattern recorded from the BCMO film in Fig. 2(a) at room temperature. No superlattice spots can be found.<sup>[7]</sup> Figure 2(c) shows a typical BF TEM image of a cross-sectional BCMO/STO sample with a film thickness of 110 nm at 103 K. The BF image was obtained under a two-beam condition with  $g = 110$ . The interface between BCMO and STO is also indicated by two arrows. Figure 2(d) displays a [ $\bar{1}\bar{1}0$ ] zone-axis SAED pattern recorded from the BCMO film at 103 K. The SAED pattern taken at 103 K is obviously different from that obtained at room temperature. It can be clearly seen from Fig. 2(d) that superlattice spots are evident in addition to the fundamental Bragg reflections. Careful examination shows that the superlattice spots exist in different directions, which could result from localized CO domains. Six different types of superlattice structures can be found in the SAED pattern, and the superlattice spots are marked by white arrows with numbers 1 to 6. The satellite spot (marked by 1) appears along the [111] direction in the reciprocal space, and the superlattice reflections exist at  $1/2$  positions between the fundamental reflections. The modulated structure can be described using a wave vector  $\mathbf{q}_1 = (1/2, 1/2, 1/2)$ , which represents a long-period structure (4.4 Å in real space) with two-fold periodicity to the original unit lattice distance. The satellite reflection (marked by 2) is along the [001] direction in the reciprocal space, and the superlattice reflections are located at  $1/2$  positions between the fundamental reflections. The wave vector of the modulated structure can be written as  $\mathbf{q}_2 = (0, 0, 1/2)$ , which represents a long-period structure (7.58 Å in real space) with two-fold periodicity to the original unit lattice distance. The satellite reflections marked by 3, 4, and 5 appear along the [110] direction in the reciprocal space, and the superlattice reflections are situated at  $1/2$ ,  $1/3$ , and  $1/5$  positions between the fundamental reflections. The wave vectors of the modulated structures can be described as  $\mathbf{q}_3 = (1/2, 1/2, 0)$ ,  $\mathbf{q}_4 = (1/3, 1/3, 0)$ , and  $\mathbf{q}_5 = (1/5, 1/5, 0)$ , which represent long-period structures with two-fold, three-fold, and five-fold periodicity to the original unit lattice distance, respectively. The periodicities of the above three modulated structures are about 5.4 Å, 8 Å, and 13.4 Å in real space, respectively. The satellite spot (marked by 6) is along the

[112] direction in the reciprocal space, and the superlattice reflections lie at  $1/12$  positions between the fundamental reflections. The wave vector of the modulated structure can be determined to be  $q_6 = (1/12, 1/12, 1/6)$ , which represents a long-period structure (18.6 Å in real space) with twelve-fold periodicity to the original unit lattice distance.

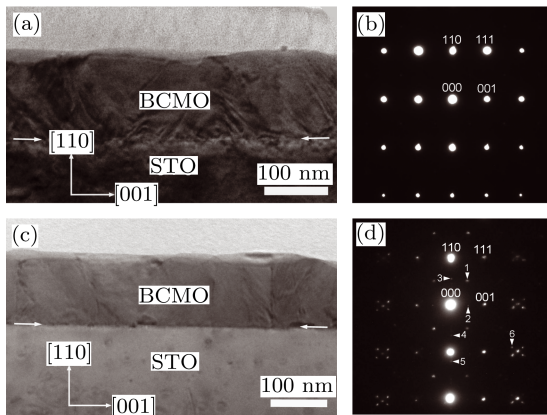


**Fig. 2.** (colour online) Cross-sectional BF image (a) and SAED pattern (b) taken at room temperature; cross-sectional BF image (c) and SAED pattern (d) obtained at 103 K.

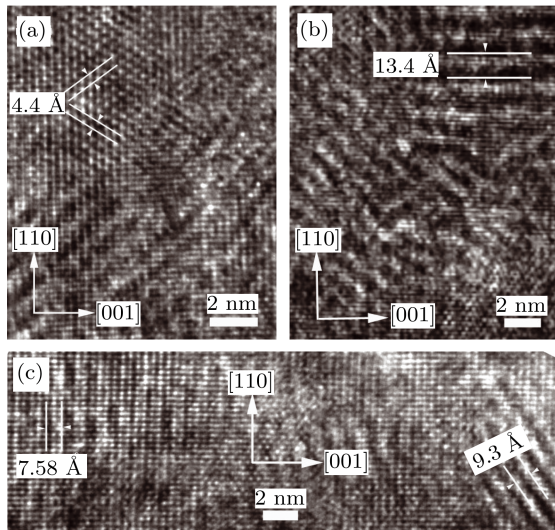


**Fig. 3.** (colour online) HRTEM images of BCMO film recorded at 103 K with localized modulations along the (a) [111] direction, (b) [110] direction, and (c) [001] and [112] direction.

To clarify the nature of the modulation, extensive HRTEM examination of the film is carried out at 103 K. HRTEM images are completely different from the results obtained at room temperature.<sup>[17]</sup> Several modulated structures are observed in the BCMO films with different modulation directions. Furthermore,

the modulation stripes are localized, and the modulation directions are not uniform. Figure 3(a) shows a typical  $[1\bar{1}0]$  zone-axis HRTEM image of the BCMO film. From the HRTEM image in Fig. 3(a), the modulated structures along the [111] direction can be found, and the modulation periodicity is about 4.4 Å. The modulated structure shown in Fig. 3(b) has a modulation periodicity of 13.4 Å and a modulation direction along the [110] direction. Figure 3(c) shows another two modulated structures in the films along the [001] and [112] direction, with periodicities of 7.58 Å and 9.3 Å, respectively. Figures 3(a) and 3(b) show the HRTEM images of the regions a little far from the STO substrate. On the contrary, figure 3(c) shows the HRTEM image of the region close to the STO substrate. In the large areas near the interface, modulated structures exist along the [001] direction with a periodicity of 7.58 Å. However, in the regions far from the interface, the modulated structure domains are small and the modulation directions are different.

In order to see the CO modulations in the films more clearly, enlarged HRTEM images are shown in Fig. 4. Figure 4(a) shows the enlarged HRTEM image of modulated stripes in the BCMO film along the [111] direction. From the enlarged image, the fringe periodicity is measured to be about 4.4 Å. Based on the SAED and HRTEM observations, structural model (after Wang *et al.*<sup>[18]</sup>) for the CO structure in Fig. 4(a) is demonstrated in Fig. 4(b). Figure 4(c) shows the enlarged HRTEM image of modulated stripes in the BCMO film along the [110] direction, and the fringe periodicity is measured to be about 13.4 Å. The structural model (after Wang *et al.*<sup>[18]</sup>) for CO structure in Fig. 4(c) is proposed in Fig. 4(d). Figure 4(e) shows the enlarged HRTEM image of modulated stripes in the BCMO film along the [001] direction. From Fig. 4(e), the fringe periodicity is measured to be about 7.58 Å, and its structural model (after Wang *et al.*<sup>[18]</sup>) for the CO state is demonstrated in Fig. 4(f). Figure 4(g) shows the enlarged HRTEM image of modulated stripes along the [112] direction, and the fringe periodicity is about 9.3 Å. The structural model (after Wang *et al.*<sup>[18]</sup>) for the CO state in the Fig. 4(g) is demonstrated in Fig. 4(h). It should be pointed out that the ratios between  $Mn^{3+}$  and  $Mn^{4+}$  in Figs. 4(b), 4(d), 4(f), and 4(h) are determined on the assumption that there is no modulation in the structure of the BCMO film along the  $[1\bar{1}0]$  direction at low temperatures.

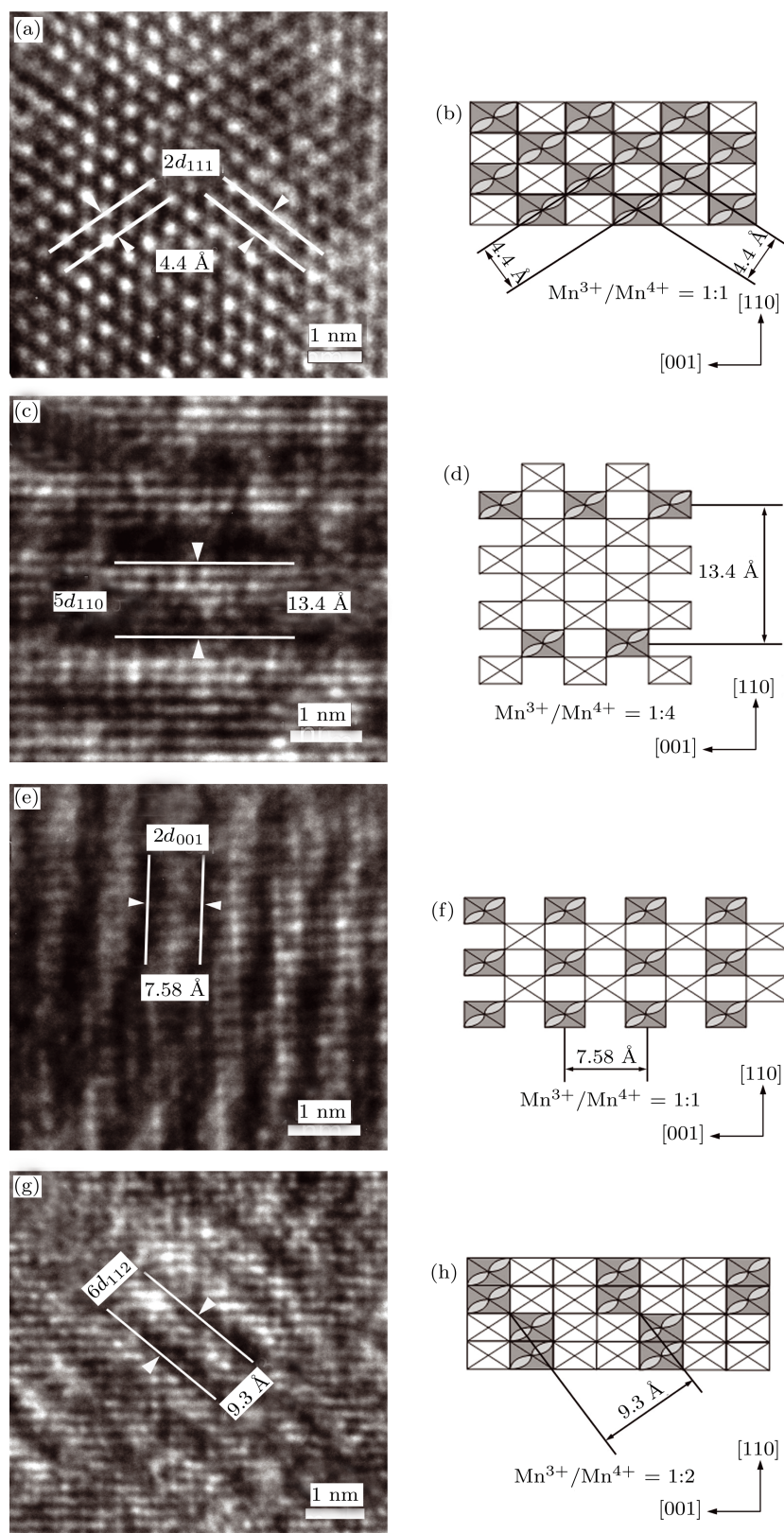


**Fig. 4.** (colour online) Enlarged HRTEM image (a) and schematic model (b) for modulation along the [111] direction; enlarged HRTEM image (c) and schematic model (d) for modulation along the [110] direction; enlarged HRTEM image (e) and schematic model (f) for modulation along the [001] direction; enlarged HRTEM image (g) and schematic model (h) for modulation along the [112] direction.  $\blacksquare$  and  $\square$  represent Mn<sup>3+</sup> and Mn<sup>4+</sup>, respectively.

It can be seen that there are six different types of superlattice spots in the SAED pattern, which appear along the [111], [110], [001], and [112] directions, respectively. The spots represent modulation periodicities of 4.4 Å, 5.4 Å, 8 Å, 13.4 Å, 7.58 Å, and 18.6 Å in real space, respectively. From the HRTEM images, it can be seen that the four different types of modulated structures are along the [111], [110], [001], and [112] directions. The modulated periodicities are measured to be 4.4 Å, 13.4 Å, 7.58 Å, and 9.3 Å, respectively. Thus, three of the spots in SAED match well with the modulated stripes in the HRTEM images. The CO stripes in HRTEM are localized and the CO domain is small. However, the selected-area aperture to obtain the SAED pattern is much bigger. That is why the SAED pattern does not completely match with the HRTEM images.

When the temperature of the BCMO films is reduced to 103 K,  $\text{Mn}^{3+}$  and  $\text{Mn}^{4+}$  will tend to be arranged in order, but the modulation direction and periodicity might vary in different locations of the epitaxial film. It should be noted that the CO is localized because the modulated structures have various periodicities and directions at different locations in the epitaxial film. The differences in modulation periodicity and direction are ascribed to the anisotropic strain in the epitaxial BCMO film. The strain plays an important role in determining the modulation direction. The strain clamps the stripes into a relatively ordered domain in the region close to the BCMO/STO interface. However, the strain becomes disordered in the region far from the interface, which will result in smaller CO domain and different modulation directions.

## 4. Conclusion

In this paper, the CO behaviours in the BCMO film with a thickness of 110 nm have been investigated at 103 K using SAED and HRTEM. The present study indicates that six different types of superlattice structures exist in the film, and three of them are confirmed

by HRTEM. It is found that the modulation periodicity and direction are completely different in the region close to the BCMO/STO interface from those in the region a little far from the BCMO/STO interface, which is attributed to the anisotropic strain in the epitaxial film. Structural models, based on the SAED and HRTEM observations, are proposed for the modulated structures in BCMO films.

## References

- [1] Tokura Y and Nagaosa N 2000 *Science* **288** 462
- [2] Lu Y, Li Q A, Di N L, Li R W, Ma X, Kou Z Q and Cheng Z H 2003 *Chin. Phys.* **12** 1301
- [3] Li R W, Sun J R, Wang Z H, Chen X, Zhang S Y and Shen B G 2000 *Chin. Phys.* **9** 630
- [4] Zou C, Chen B, Zhu X J, Zuo Z H, Liu Y W, Chen Y F, Zhan Q F and Li R W 2011 *Chin. Phys. B* **20** 117701
- [5] Li J Q, Chen L, Yu H C, Matsui Y and Zhao Z X 2003 *Chin. Phys. Lett.* **20** 738
- [6] Wang R H, Gui J N, Zhu Y M and Moodenbaugh A R 2001 *Phys. Rev. B* **63** 144106
- [7] Li J Q, Matsui Y, Kimura T and Tokura Y 1998 *Phys. Rev. B* **57** R3205
- [8] Li G, Tang A N, Yang Y, Wang W, Li X G, Wang Z D and Ku H C 2003 *Appl. Phys. Lett.* **83** 5250
- [9] Lu W J, Sun Y P, Zhao B C, Zhu X B and Song W H 2006 *Phys. Rev. B* **73** 214409
- [10] Smolyaninova V N, Talanova E, Kennedy R, Kolagani Rajeswari M, Overby M, Aldaco L, Yong G and Karki K 2007 *Phys. Rev. B* **76** 104423
- [11] Bao W, Axe J D, Chen C H and Cheong S W 1997 *Phys. Rev. Lett.* **78** 543
- [12] Woo H, Tyson T A, Croft M, Cheong S W and Woicik J C 2001 *Phys. Rev. B* **63** 134412
- [13] Kim D H, Christen H M, Varela M, Lee H N and Lowndes D H 2006 *Appl. Phys. Lett.* **88** 202503
- [14] Chen Y Z, Sun J R, Liang S, Lü W M, Shen B G and Wu W B 2008 *J. Appl. Phys.* **103** 096105
- [15] Chen Y Z, Sun J R, Wang D J, Liang S, Wang J Z, Han Y N, Han B S and Shen B G 2007 *J. Phys.: Condens. Matter* **19** 442001
- [16] Chen Y Z, Sun J R, Liang S, Lü W M and Shen B G 2008 *J. Appl. Phys.* **104** 113913
- [17] Ding Y H, Cai R S, Du Q T, Wang Y Q, Chen Y Z and Sun J R 2011 *J. Cryst. Growth* **317** 115
- [18] Wang Y Q, Duan X F, Wang Z H and Shen B G 2001 *Appl. Phys. Lett.* **78** 2157